Analyst

RSC Publishing

PAPER

View Article Online
View Journal



# Nitrogen-doped zinc oxide thin films biosensor for determination of uric acid

Cite this: DOI: 10.1039/c3an36695b

Kajal Jindal,[a] Monika Tomar[b] and Vinay Gupta*[a]

Nitrogen-doped zinc oxide thin films (ZnO:N) have been realized as a potential matrix for the development of a uric acid biosensor. The correlation between the change in property of the ZnO film with N doping concentration and its biosensing response has been studied. The nitrogen dopant in a ZnO film alters its defects profile, thus improving the charge transfer characteristics and resulting in an enhanced peak oxidation current in the cyclic voltammogram in comparison to that of the pure ZnO film. The studies reveal that the bio-electrode based on the nitrogen-doped ZnO thin film matrix exhibits better sensitivity (1.1 mA $mM^{-1}$ $cm^{-2}$) with linearity over a wide range (0.05 mM to 1.0 mM) of uric acid concentration. A comparatively low value (0.10 mM) of the Michaelis–Menten constant ($K_m$) indicates high affinity of the immobilized uricase towards uric acid. The proposed ZnO:N thin films matrix-based uric acid-biosensor has good reproducibility, a long shelf-life (20 weeks) and high selectivity.

Received 15th November 2012
Accepted 16th April 2013

DOI: 10.1039/c3an36695b

www.rsc.org/analyst

## Introduction

Uric acid is one of the primary end products of purine metabolism in the human body. Fast and accurate determination of its level dissolved in human physiological fluids has been recognized as a vital clinical test in the diagnosis of patients suffering from numerous metabolic disorders originating due to altered purine biosynthesis and catabolism such as gout, arthritis, neurological, cardiovascular and kidney diseases. Thus, continuous monitoring of uric acid levels in the blood is of paramount importance. In recent years, many efforts have been paid to develop reliable uric acid biosensors using electrochemical,[1] chemiluminescence[2] or other methods.[3] Among all the methods, the enzyme-based electrochemical uric acid biosensor has drawn the main interest within biosensor research owing to its unique features including high sensitivity, high selectivity, relatively low cost and simple operation.[4] Since the performance of a biosensor is highly dependent on the matrix used for immobilization, choice of a suitable matrix that facilitates the immobilization of the biomolecule with the desired conformation that retains its activity is crucial for the realization of sensitive and stable biosensors.[5]

Most of the efforts for the development of uric acid biosensor are directed towards the immobilization of uricase onto polymer thin films,[3,6–14] which suffers from the problem of fast degradation in response characteristics with time and thus limits their application for *in vivo*-monitoring. Ahuja *et al.*[1] reported the amperometric detection of uric acid based on the immobilization of uricase onto an APTES/ITO electrode *via* the crosslinker, BS[3], but the sensitivity of the developed sensor was low (39.35 μA $mM^{-1}$). Pan *et al.*,[15] in another report, investigated the sensing performance of a uric acid biosensor based on a copolymer of *o*-aminophenol–aniline and inferred that the sensitivity degraded by 15% in just 15 days. He *et al.*[16] studied the electrochemistry of a quercetin-modified wax-impregnated graphite electrode used for the biosensing of uric acid, but long-term stability was poor as the sensor was found to degrade (10% decrease in activity) within a month. Chen *et al.*[14] employed a molecularly imprinted polymer thin film as a biosensor for uric acid and observed that the sensitivity of the biosensor was dependent on the thickness of the polymer film where the sensitivity is at a maximum (24.72 μA $mM^{-1}$) with 0.6 wt% of polymer. Surprisingly, only a few reports are available on the utilization of metal oxide matrices for the analysis of uric acid that are well known for their remarkable stability, easy preparation and excellent charge transfer characteristics.[17] Among all the metal oxide matrices, zinc oxide (ZnO), being a wide band gap semiconductor (~3.37 eV) with a high exciton binding energy (60 meV), finds multifunctional applications due to its exciting properties such as biocompatibility, good electron communication feature, high isoelectric point (~9.0), good electrochemical properties, simple and cost effective synthesis, non-toxicity, high optical transparency in the visible region, and so forth.[18,19] ZnO thin films are the most extensively researched matrix for the development of various biosensors for the detection of glucose,[20] cholesterol,[21] $H_2O_2$,[22] DNA,[23] urea,[24] uric acid[25] *etc.* due to its unmatched stability and reproducibility. However, the only setback that limits its further advancement in the field of biosensors is its limited charge transfer feature, leading to low sensitivity in comparison to other inorganic matrices such as NiO,[26] $ZrO_2$,[27] *etc*. Efforts have been made to

[a]*Department of Physics and Astrophysics, University of Delhi, Delhi 110007, India. E-mail: vgupta@physics.du.ac.in; Tel: +91-9811563101*

[b]*Department of Physics, Miranda House, University of Delhi, Delhi 110007, India*

improve the sensitivity of ZnO-based biosensor by making hybrid composite matrices.[23,28,29]

ZnO is an n-type semiconductor due to the presence of native defects related to oxygen vacancies and shallow zinc interstitials.[30] It is well known that doping can effectively tailor the functional properties of ZnO[31,32] and exploitation of a single-phase material is advantageous for reproducible device applications. However, it is important to point out that no efforts have been made to engineer the properties of ZnO *via* doping in order to improve the charge transfer characteristics which may lead to much simpler and stable bio-electrodes. Among various dopants in ZnO, nitrogen (N) has attracted particular interest due to its interesting properties.[33,34] The ionic radius of N is very close to that of O.[35] Nitrogen doping is well known to alter the electrical conductivity of ZnO[36] and alter the band gap.[37] The appropriate doping of N can produce electronic defects[34] which may enhance the charge transfer capability of the matrix (ZnO) and improve its sensitivity and stability. Despite the use of nitrogen-doped ZnO (ZnO:N) in a wide variety of applications, its applicability in biosensing has never been explored which may offer a novel route for obtaining biosensors with improved response characteristics.

In the present work, a highly sensitive uric acid biosensor has been developed using a nitrogen-doped ZnO thin film deposited by pulsed laser deposition. Amount of N doping in the ZnO matrix has been optimized to obtain an efficient biosensor for the detection of uric acid.

## Experimental

### Reagents and solutions

Uric acid (99.99% pure), uricase (E.C.1.7.3.3 from *Candida* sp.), horseradish peroxidase (HRP) and *o*-dianisidine dye were purchased from Sigma-Aldrich. Sodium phosphate monobasic anhydrous and sodium phosphate dibasic dihydrate (analytical reagent grade) were obtained from Sisco chemical, India. All these chemicals were used without any additional purification. Deionized water (resistivity = 18.2 MΩ cm) was used for the preparation of aqueous solutions.

A 50 mM phosphate buffer saline (PBS) solution was freshly prepared by mixing stock solutions of monosodium dihydrogen phosphate ($NaH_2PO_4$) and disodium hydrogen phosphate ($Na_2HPO_4$). 0.9% Sodium chloride (NaCl) was added to the prepared solution in order to adjust its pH to 7. The prepared solution was used as an electrolyte for the electrochemical measurements. Enzyme solution (uricase: 1 mg ml$^{-1}$, 4.9 U) was prepared by dissolving the enzyme in the prepared PBS solution. Different concentrations of uric acid solution (0.05–3.0 mM) and solution of *o*-dianisidine (1%) dye were freshly prepared in de-ionized water.

### Preparation of ZnO:N thin film-based electrode and immobilization of uricase

ZnO and ZnO:N thin films were grown by a Pulsed Laser Deposition (PLD) technique using the fourth harmonic of a Nd:YAG laser ($\lambda$ = 266 nm). Ceramic targets of one inch diameter of $ZnO_{1-x}N_x$ with variable N doping concentrations ($x$ = 0, 0.02, 0.04, 0.08 and 0.10) were prepared by a conventional solid-state reaction method.[38] The high purity powders of ZnO (99.999% purity) and $Zn_3N_2$ (99.999% purity) were taken in appropriate amounts by varying wt% and were mixed for 24 hours through ball milling with zirconia balls. The mixed powder was sieved and calcined at 600 °C for 5 hours. The calcined powder was then pressed into the form of a pellet using a die under a pressure of 3.0 Torr using a hydraulic press, and the prepared pellets were sintered at 900 °C for 5 hours to obtain the dense ceramic targets of $ZnO_{1-x}N_x$ of the respective compositions. Thin films were deposited onto ITO-coated glass substrates (commercially available) by ablating the respective target in an oxygen-rich environment (100 mTorr) at a fluence of 1.2 J cm$^{-2}$ and a repetition rate of 10 Hz. The deposition chamber was evacuated to a base pressure of $2 \times 10^{-6}$ Torr, prior to the deposition. Deposition of thin films was carried out at room temperature and a target-to-substrate distance of 5 cm was maintained. A number of laser pulses were applied in order to keep the thickness of the ZnO and ZnO:N thin films fixed at about 90 nm. It may be noted that the dopant N has been incorporated into the target material according to the wt% of dopant. Since, the deposition of ZnO:N thin films has been carried out using the PLD technique which is known to maintain the stoichiometry of the material, the concentration of N doping in the ZnO:N thin film is assumed to be same as that in the ZnO:N ceramic targets. It may be noted that an area of 2 cm × 1 cm of ITO-coated glass is taken for the fabrication of biosensor. However, the $ZnO_{1-x}N_x$ thin film is grown on an area of 1 cm × 1 cm using a shadow mask. The remaining uncovered lower conducting ITO layer (*i.e.* (1 cm × 1 cm area)) serves as an electrode and is used for taking out electrical connections. In order to prepare the bio-electrode, 10 μl (0.049 U) of the freshly prepared uricase solution (1 mg ml$^{-1}$ in PBS solution) is drop-casted onto the surface of the ZnO:N/ITO/glass electrode so as to immobilize the uricase electrostatically *via* a physical adsorption technique. The bio-electrode was kept overnight for drying. Thereafter, the prepared bio-electrode (uricase/ZnO:N/ITO/glass) was extensively rinsed with PBS buffer to remove any excess loosely bound uricase. The bio-electrode was dried under nitrogen flow and stored at 4 °C when not in use. The schematic of the prepared bio-electrode is shown in Fig. 1.

### Measurement and apparatus

The crystalline structure and phase of the prepared ZnO and ZnO:N thin films was identified by the X-ray Diffraction (XRD)

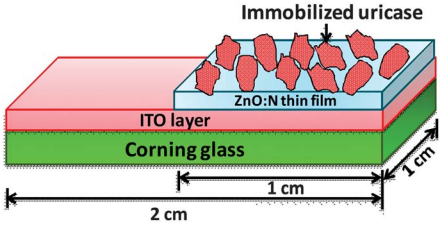


**Fig. 1** Schematic representation of the prepared uricase/ZnO:N/ITO/glass bio-electrode.

technique (Bruker D8). The film thickness was determined using a surface profiler (Dektak 150A). The surface morphology of the prepared ZnO:N/ITO/glass electrode and uricase/ZnO:N/ITO/glass bio-electrode was investigated using atomic force microscopy (AFM) (Veeco DICP2). An FTIR spectrophotometer (Perkin Elmer; Model Spectrum BX) was used to confirm the enzyme immobilization. To study the electrochemical properties of the bio-electrode, cyclic voltammetric measurements were carried out using a Potentiostat/Galvanostat (Gamry Inc. 600) having a three-electrode electrochemical cell configuration with Ag/AgCl serving as reference electrode, platinum foil as counter electrode and uricase/ZnO:N/ITO/glass as working electrode. PBS solution (10 ml, 50 mM, 0.9% NaCl) containing a mediator of 5 mM $K_3[Fe(CN)_6]$ was used as electrolyte. The apparent enzyme activity of the prepared uricase/ZnO:N/ITO/glass bio-electrode was determined using a UV-visible spectrophotometer (Perkin Elmer: lambda 35). All the experiments in the present study were performed in accordance with the relevant laws and institutional guidelines.

## Results and discussion

### Structural studies

The XRD pattern of the ZnO:N thin films deposited using PLD is shown in Fig. 2. The (002) diffraction peak corresponding to the wurtzite structure of ZnO is observed to be the dominant peak in all deposited thin films, revealing the growth of preferred oriented ZnO:N thin films with the *c*-axis normal to the substrate. The pure ZnO thin film exhibits (002) diffraction at $2\theta \approx 33.94^\circ$, which is smaller in comparison to the corresponding unstressed value of 34.42° reported for bulk ZnO[39] and reveals the presence of stress in the deposited thin film. However, on introducing N into the ZnO lattice (with $x = 0$–0.10), a continuous decrease in the value of $2\theta$ for the (002) diffraction peak from 33.94° to 33.78° is observed (Fig. 2, Table 1). The values of the *c*-axis and *a*-axis length have been calculated from the $2\theta$ values corresponding to the (002) and (102) plane respectively. The estimated values of the *c*-axis and *a*-axis length for all prepared $ZnO_{1-x}N_x$ thin films using XRD studies are presented in Table 1. The *c*-axis length is found to increase from 5.278 Å for the pure ZnO thin film to about 5.302 Å for 10% N doping in ZnO. Thus, it is inferred that N doping causes an expansion in the ZnO unit cell along the *c*-axis. This expansion in the lattice upon N doping in ZnO is in agreement with previous reports on N-doped ZnO.[40] Since, the ionic radius of $N^{3-}$ is slightly larger than the ionic radius of $O^{2-}$,[35] the expansion in the lattice along the *c*-axis with increase in N dopant concentration indicates that N atoms are substituting the O lattice sites in the ZnO lattice.[40] Also, it may be noted that the full width at half maximum (FWHM) of the (002) diffraction peak is found to increase with an increase in N doping concentration which implies a decrease in crystallinity with N doping. The average size of the crystallite (*D*) has been calculated from the FWHM of the (002) diffraction peak using Scherrer's relation.[39] All the deposited thin films (ZnO and ZnO:N) are found to be nanocrystalline with crystallite sizes in the range of 10–15 nm. However, the average crystallite size (*D*) is found to decrease from 15 nm (ZnO) to 10 nm with the incorporation of N (10%) into the ZnO lattice and is attributed to an enhancement in disordering in the ZnO film as a result of the N doping.[41] The Lotgering factor has been calculated for the prepared ZnO and ZnO:N thin films using the recorded XRD spectra in order to determine the degree of orientation.

The Lotgering factor, *f*, for the (00l) family of planes is given by:[42]

$$f_{00l} = \frac{P_{00l} - P_0}{1 - P_0}$$

where

$$P_{00l} = \frac{\sum I_{00l}}{\sum I_{hkl}}$$

and

$$P_0 = \frac{\sum I^0_{00l}}{\sum I^0_{hkl}},$$

where $I_{hkl}$ and $I^0_{hkl}$ are the intensities of (*hkl*) peaks for the textured and randomly oriented sample (JCPDS file no. 36-1451). The calculated values of the Lotgering factor for the prepared ZnO:N thin films are given in Table 1. It may be noted that the values of Lotgering factor *f* for all the prepared thin films are very close to 1 which indicates that all prepared pure ZnO and doped ZnO:N thin films are preferred oriented along (002) plane. The obtained values are in agreement with the ones reported in the literature for ZnO thin films ($f = 0.98$,[43] $f = 0.90$[44]). Also, the incorporation of N is not found to affect the crystallographic orientation of the deposited films and may be attributed to the small difference in the ionic radii of N and O which may preserve the structure of the host ZnO lattice.

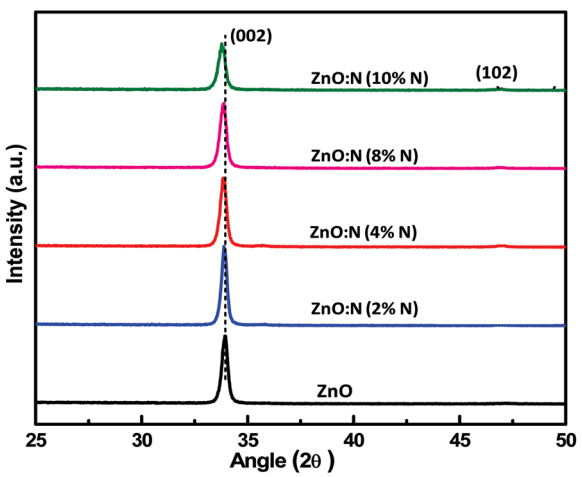


**Fig. 2** XRD spectra of the as-deposited ZnO and ZnO:N thin films having different concentrations of N dopant.

### Surface morphology

The surface morphology of the bare ITO electrode and the deposited ZnO:N thin film before and after enzyme immobilization is investigated using atomic force microscopy (AFM) and

**Table 1** Structural parameters and surface roughness of the deposited $ZnO_{1-x}N_x$ thin films

| N concentration $x$ in $ZnO_{1-x}N_x$ | $2\theta$ for (002) reflection (°) | Lattice constant, $c$/Å | Lattice constant, $a$/Å | Crystallite size/nm | Lotgering factor, $f$ | Surface roughness/nm |
|---|---|---|---|---|---|---|
| 0 | 33.94 | 5.278 | 3.219 | 15 | 0.962 | 4 |
| 0.02 | 33.91 | 5.282 | 3.216 | 14 | 0.963 | 5 |
| 0.04 | 33.89 | 5.285 | 3.214 | 13 | 0.968 | 6 |
| 0.08 | 33.85 | 5.291 | 3.213 | 12 | 0.974 | 9 |
| 0.10 | 33.78 | 5.302 | 3.205 | 10 | 0.977 | 10 |
| ZnO (bulk)[37] | 34.43 | 5.2066 | 3.249 | — | 0 | — |

the images are shown in Fig. 3(a)–(g). The AFM image of the bare ITO electrode (Fig. 3(a)) shows a smooth surface, whereas a rough surface with uniformly distributed grains can be seen in the AFM images of the ZnO:N thin film (Fig. 3(b)–(f)). The rough surface morphology of the ZnO:N thin film is beneficial for efficient loading of the enzyme on its surface.[45,46] Also, it may be clearly inferred from Fig. 3(b)–(f) that there is a decrease in the grain size of the ZnO:N thin films prepared using targets with an increase in N doping from pure ZnO to 10%. This is in agreement with the XRD studies which demonstrate a decrease in crystallite size with N doping (Table 1). The decrease in grain size results in an increase in the surface-to-volume ratio and grain boundaries. The increase in surface area leads to an increased enzyme (uricase) loading on the surface of the deposited ZnO:N thin film. Upon loading the ZnO:N thin film with uricase, clusters of uricase bio-molecules forming a globular structure of much bigger size (~2 μm) may be seen in Fig. 3(g). This indicates the successful immobilization of enzyme (uricase) onto the surface of the ZnO:N/ITO/glass electrode. The average surface roughness for the deposited ZnO:N thin films is estimated using AFM studies and is found to increase from 4 to 10 nm with an increase in N doping concentration from 0 to 10 wt% in the ZnO:N target. Table 1 lists the values of the surface roughness for the deposited ZnO:N thin films. The increase in surface roughness of the ZnO:N thin film is also beneficial for efficient loading of the enzyme, thus leading to higher peak currents in cyclic voltammetry (Fig. 4). This is in agreement with previous reports where an increase in enzyme loading is observed with an increase in surface roughness.[45,46] The average root mean square (rms) roughness of the ZnO:N (8 wt% N) thin film surface is found to increase from 9 nm to 36 nm after the immobilization of uricase.

## Electrochemical property

Fig. 4 shows the effect of N doping concentration (0–10 wt%) on the cyclic voltammetric (CV) response of the ZnO:N/ITO/glass electrode. Well aligned CV spectra were obtained for all electrodes based on ZnO:N matrices and the oxidation current peak was observed at a potential of about 0.45 V. It may be seen from Fig. 4 that as the concentration of N dopant in the ZnO thin film increases, the peak oxidation current keeps on increasing, having a maximum value of 1.65 mA for an 8 wt% N-doped ZnO thin film matrix. The value of the peak oxidation current reduces to 1.5 mA with further increase in concentration of N dopant to 10 wt% in the ZnO thin film. The increase in peak oxidation current with N doping concentration may be related to two factors. Firstly, XRD spectra (Fig. 2) demonstrate a decrease in crystallite size with increasing N doping concentration. The smaller crystallites in the ZnO:N thin film provide increased surface area for efficient loading of enzyme.[26,45,46] Also, AFM images shown in Fig. 3(b)–(f) reveal a decrease in grain size of the ZnO:N thin films prepared using targets with an increase in N doping from pure ZnO to 10 wt%. The decrease in grain size results in an increase in the surface-to-volume ratio and grain boundaries. The increase in surface area leads to an increased enzyme (uricase) loading on the surface of the deposited ZnO:N thin film.[46] Thus, the observed enhancement in the current response with increase in N doping concentration in ZnO is attributed to the increased concentration of electroactive uricase on the surface of the ZnO:N thin film. A higher number of electroactive enzyme (uricase) molecules leads to increased oxidation and reduction currents, in the presence of a fixed concentration of analyte (uric acid), thereby, enhancing the sensitivity and the biosensing response. Secondly, N doping induces defect states in the ZnO band gap, leading to improved electron communication features. The decrease in peak oxidation current for higher N doping ($x = 0.10$) within the ZnO thin film may be attributed to the accumulation of N at the interstitial sites, which creates steric hindrance, thus obstructing the flow of charge carriers.[47,48] The exact location of introduced nitrogen at either the substitutional or interstitial sites in the host ZnO lattice is unclear. However, at low concentrations of nitrogen (N) dopant, N is expected to substitute at the oxygen sites due to low formation energy, resulting in an improved sensitivity. At higher doping concentrations, the possibility of incorporation of N at interstitial sites may not be ruled out.[48] The wurtzite structure of ZnO has two interstitial sites: tetrahedral and octahedral. Interstitial nitrogen is unlikely to occur at octahedral sites due to the high formation energy,[48] whereas, they are unstable at tetrahedral sites and spontaneously relax into a kick out configuration, where both oxygen and nitrogen atoms share the same lattice site.[48] Further, it is reported that interstitial nitrogen at tetrahedral sites traps more electrons in comparison to oxygen.[48] Therefore, a saturation in the peak oxidation current is observed due to hindrance of the flow charge carriers by the interstitial nitrogen. Thus, an N-doped ZnO thin film having a maximum peak oxidation current with a doping concentration of 8 wt% was used for further investigations based on the development of uric acid biosensor.

 

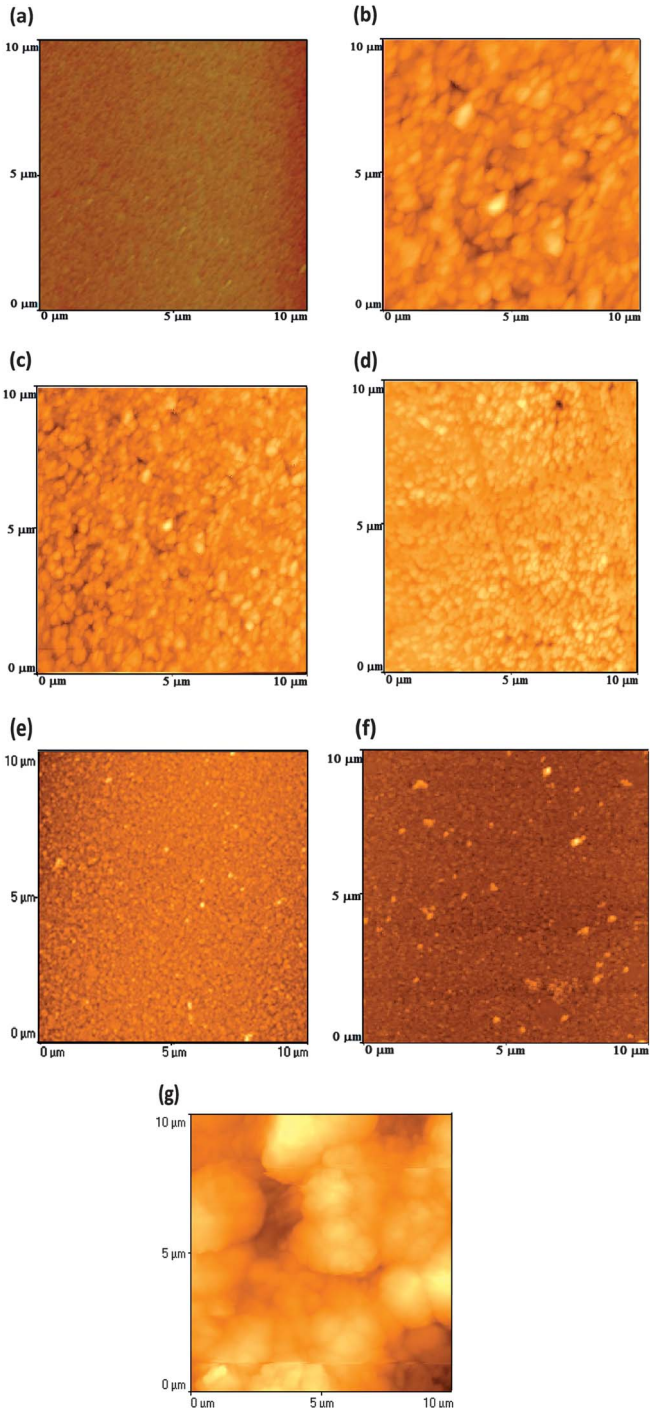


**Fig. 3** AFM images of the (a) bare ITO electrode; ZnO:N/ITO/glass electrode with varying concentrations of N doping: (b) 0% (ZnO), (c) 2%, (d) 4%, (e) 8%, (f) 10%, and (g) uricase immobilized on 8% N-doped ZnO thin film (uricase/ZnO:N/ITO/glass bio-electrode).

## FTIR studies

ZnO:N thin films were grown on Si substrates and characterized by FTIR spectroscopy in the range of 400–4000 $cm^{-1}$ before and after immobilization of the enzyme and the corresponding spectra are shown in Fig. 5. The IR spectrum of the ZnO:N thin film shows the characteristic absorption bands of ZnO at 457 and 567 $cm^{-1}$ (Fig. 5) which originates from the stretching mode of the Zn–O bond and confirms that N is substituting well at the O lattice sites within the wurtzite structure of ZnO.[49] The presence of the enzyme (uricase) on the surface of the

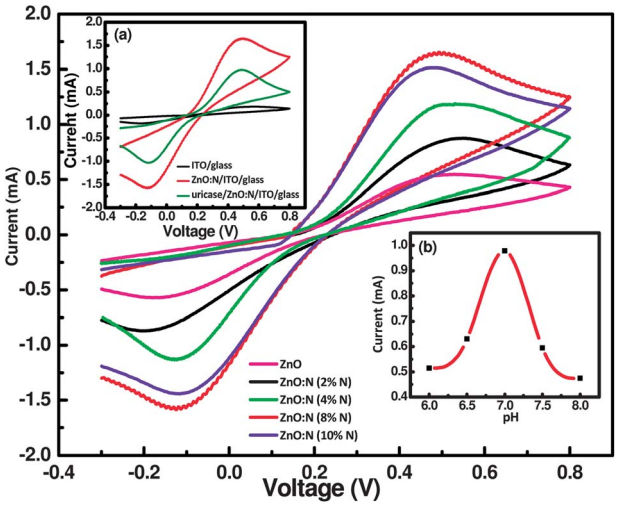


**Fig. 4** CV spectra of ZnO and ZnO:N thin films as a function of N doping concentrations ($x = 0$–$0.10$) (scan rate = 100 mV $s^{-1}$). Inset (a) shows the cyclic voltammetry response of the ITO/glass electrode, ZnO:N ($x = 0.08$)/ITO/glass electrode and uricase/ZnO:N ($x = 0.08$)/glass bio-electrode. Inset (b) shows the effect of pH on the peak oxidation current of the uricase/ZnO:N/ITO/glass bio-electrode.

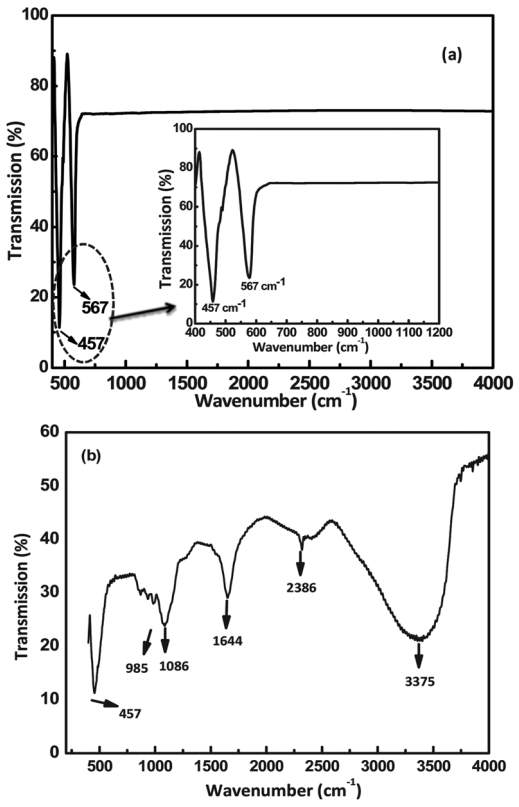


**Fig. 5** FTIR spectra of (a) ZnO:N thin film (inset shows the enlarged image) and (b) ZnO:N thin film upon immobilization with uricase.

ZnO:N/ITO/glass electrode is revealed by the appearance of additional absorption bands at 985, 1086, 1644, 2386 and 3375 $cm^{-1}$ (Fig. 5). The bands at 985 $cm^{-1}$ and 1086 $cm^{-1}$ correspond to the C–H bonding of alkene and C–N vibrations. The mode at 1644 $cm^{-1}$ and a broad absorption peak at 3375 $cm^{-1}$ correspond to the O–H bending band, which is associated with the adsorbed water molecules on the surface of the thin film sample.[5] Thus, the FTIR studies confirm the presence of uricase on the surface of the ZnO:N thin film matrix. However, it could be noted that uricase has been immobilized on the surface of the prepared matrix *via* electrostatic interactions which may not be confirmed by FTIR.

### Biosensing response characteristics

CV curves were obtained for ITO/glass, ZnO:N/ITO/glass and uricase/ZnO:N/ITO/glass ($x = 0.08$) electrodes and are shown in the inset (a) of Fig. 4. It may be clearly seen that the peak oxidation current of the deposited ZnO:N thin film-based electrode (1.65 mA) is higher in comparison to that of the bare ITO/glass electrode (0.20 mA) despite the fact that ITO, being a transparent conducting oxide, has a higher electrical conductivity than that of semiconducting ZnO:N. This may be due to the fact that the conductivity of the thin film is not a key parameter for biosensing applications. It is the quality and surface area of the thin film which play a crucial role for effective and conformal immobilization of the enzyme in addition to its high electron communication features that affect the biosensing response to a large extent.[26] The study indicates the good electrochemical properties of the ZnO:N thin film deposited in the present study. The value of the peak oxidation current obtained for the ZnO:N thin film-based matrix was found to be enhanced in comparison to that reported for other matrices used for uric acid biosensing, such as the nano-Au/PPyox/GCE electrode,[11] quercetin-modified wax-impregnated graphite electrode,[16] SAM of PET and DTB on gold[50] and $BS^3$/APTES/ITO/glass electrode.[1] The high value of current obtained in the ZnO:N thin film-based electrode may be attributed to the defects that have arisen due to N doping, thus acting as an electron transfer channel. The magnitude of the peak oxidation current is found to decrease considerably on immobilization of uricase on the surface of the prepared ZnO:N/ITO/glass electrode (0.95 mA). This is attributed to the formation of a non-conducting layer of uricase enzyme on the electrode surface, which obstructs the transfer of electrons. The pH of the supporting electrolyte is known to have a significant influence on the peak oxidation current.[26,51] The response of the prepared uricase/ZnO:N/ITO/glass bio-electrode was investigated over a range (6.0 to 8.0) of pH of the supporting buffer solution in order to ascertain the optimal working conditions. The dependency of the pH of the buffer on the peak oxidation current of the bio-electrode is shown in inset (b) of Fig. 4. The biosensing response current was found to increase with an increase in pH from 6.0 to 7.0 where it exhibits a maximum (pH 7.0) and decreases thereafter. So, PBS solution at pH 7.0 was chosen for use in the present experiment.

In order to further analyse the kinetic and transfer characteristics of the prepared uricase/ZnO:N/ITO/glass bio-electrode, CV measurements were carried out at different scan rates varying from 80 mV $s^{-1}$ to 170 mV $s^{-1}$ as shown in Fig. 6. It is interesting to note from Fig. 6 that with an increase in the scan rate, the separation between the anodic ($E_{pa}$) and cathodic peak potential ($E_{pc}$) values for the bio-electrode increases, implying the quasi-reversible behaviour of the system.[52] Inset (a) of Fig. 6 gives the variation in peak oxidation and reduction current as a function of scan rate. It may be seen that both the oxidation and reduction peak currents of the uricase/ZnO:N/ITO/glass bio-electrode vary linearly with the scan rate, implying that a surface-controlled electrochemical process is taking place at the bio-electrode. The surface concentration of ionic species per unit area for the uricase/ZnO:N/ITO/glass bio-electrode is estimated using the Brown–Anson model.[53] The estimated value of surface concentration of electroactive uricase is found to be about $8.22 \times 10^{-7}$ mol $cm^{-2}$ which is greater in comparison to the corresponding values reported by other workers for uric acid sensors.[11] The increased value of surface concentration obtained in the present work confirms that the ZnO:N/ITO/glass bio-electrode exhibits a high enzyme loading owing to the high surface area of the ZnO:N thin film, which is advantageous for improved sensitivity of the developed biosensor.

The electrochemical sensing response of the prepared uricase/ZnO:N/ITO/glass bio-electrode towards uric acid has been investigated. The physiological range of uric acid in human serum is between 0.13 and 0.46 mM.[54] Thus, the concentration of uric acid (analyte) was varied from 0.05 to 3.0 mM in the electrolyte solution and the corresponding CV spectra were recorded as shown in Fig. 7. In order to evaluate the reproducibility of the developed ZnO:N thin film-based biosensor, repetitive CV measurements were carried out and the relative standard deviation (R.S.D) in the measurement of the peak oxidation current with subsequent addition of uric acid was calculated. The obtained results are summarized in Table 2. It

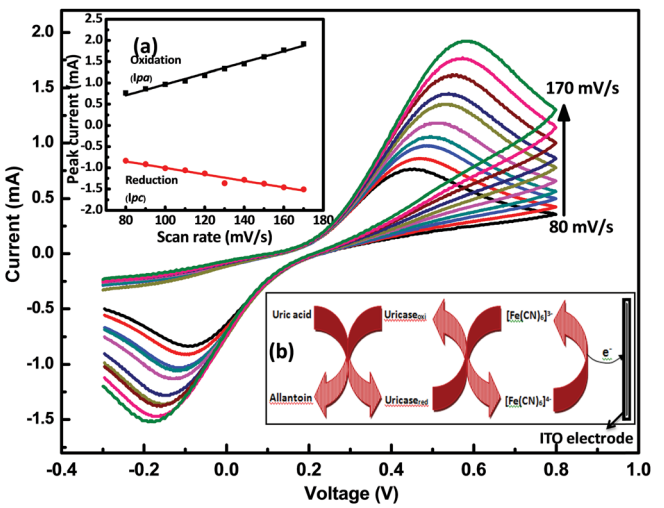


**Fig. 6** CV spectra of the uricase/ZnO:N/ITO/glass bio-electrode in PBS solution as a function of scan rate varied from 80 to 170 mV $s^{-1}$. Inset (a) gives the variation in anodic ($I_{pa}$) and cathodic ($I_{pc}$) peak currents as a function of scan rate. Inset (b) gives the schematic of the electron transfer taking place at the uricase/ZnO:N/ITO/glass bio-electrode in the presence of uric acid.

may be observed from Fig. 7 that the oxidation peak current increases from 0.983 mA to 2.04 mA with increase in the uric acid concentration from 0.05 to 1.0 mM and saturates thereafter (2.10 mA) for values ≥2.0 mM uric acid concentration. In addition, the currents measured in three repeated measurements give an R.S.D. of between 1 and 3%, which highlights the excellent reproducibility of the prepared bio-electrode in the sensing measurements. Uricase reacts with uric acid and converts it into allantoin. During re-oxidation of uricase after the enzymatic reaction, the mediator ($K_3[Fe(CN)_6]$) accepts an electron and gets reduced. The reduced form is reoxidized at the electrode surface, thus producing electrons. These electrons are then transferred to the lower ITO layer through the ZnO:N thin film matrix, thus completing the conduction path. The catalytic oxidation of uricase increases as the concentration of uric acid in the electrolyte increases, which thereby results in the release of more electrons, giving a current signal proportional to the uric acid concentration. The schematic of the electron transfer taking place at the uricase/ZnO:N/ITO/glass bio-electrode in the presence of uric acid is shown in inset (b) of Fig. 6. It may be noted that both the oxidation and reduction peaks increase simultaneously with the concentration of uric acid. However, this simultaneous increase may be understood from the fact that as the potential is swept back and forth, a current flows through the electrode that either oxidizes or reduces the analyte. The analyte (uric acid) is oxidized during the initial sweep to form the product (allantoin) but during the return sweep product is reduced back to its original form. Therefore, as the concentration of analyte (uric acid) increases, both the oxidation and reduction peaks increase because one process is anodic and the other is cathodic. A saturation in the peak oxidation current obtained for 2.0 mM uric acid concentration may be attributed to the fact that no more active sites are present for further binding of the substrate (uric acid). The developed ZnO:N thin film-based biosensor exhibits good linearity over the measured range of uric acid concentration (0.05 to 1.0 mM) (inset (a) in Fig. 7) and follows the regression equation:[55]

Peak current (mA) = 1.1 × uric acid concentration (mM) + 0.9366 ($R$ = 0.998, S.D. = 0.018 mA) (1)

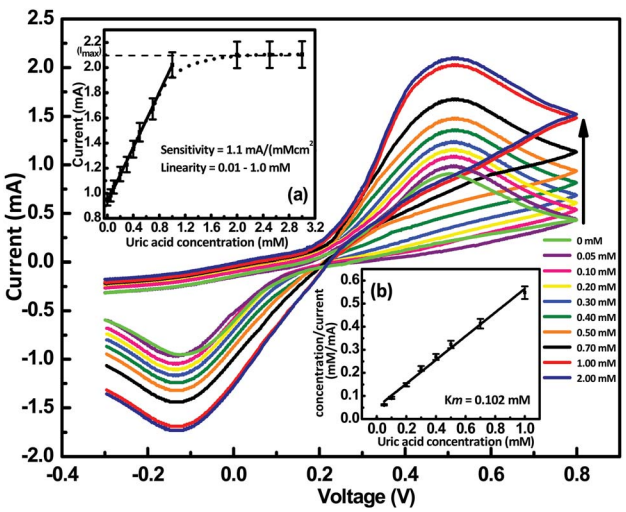


**Fig. 7** Sensing response of the uricase/ZnO:N/ITO/glass bio-electrode as a function of uric acid concentration (0.05–2.0 mM). Inset (a) gives the variation in peak oxidation current with uric acid concentration and (b) Hanes plot.

**Table 2** Electrochemical response of the developed ZnO:N thin film-based biosensor towards uric acid

| Concentration of uric acid added/mM | Measured current/mA | R.S.D. ($n$ = 3) (%) |
|---|---|---|
| 0 | 0.950 | 1.02 |
| 0.05 | 0.983 | 1.10 |
| 0.1 | 1.050 | 1.33 |
| 0.2 | 1.154 | 1.49 |
| 0.3 | 1.229 | 1.86 |
| 0.4 | 1.352 | 2.12 |
| 0.5 | 1.487 | 2.36 |
| 0.7 | 1.672 | 2.53 |
| 1.0 | 2.040 | 2.72 |
| 2.0 | 2.100 | 2.99 |

The sensitivity of prepared biosensor towards uric acid has been calculated from the slope of the linear portion of calibration curve (inset (a) in Fig. 7) and is found to be 1.1 mA $mM^{-1}$ $cm^{-2}$. The results indicate that the ZnO:N thin film-based uric acid biosensor is more sensitive (1.1 mA $mM^{-1}$ $cm^{-2}$) in comparison to those reported in the literature in the range of 3–40 μA $mM^{-1}$ for other metal oxides-based uric acid biosensors.[1,4,14,50] Also, it is important to mention that the sensitivity of the bio-electrode prepared using the ZnO thin film matrix deposited under similar conditions in the present case is almost one-third of that obtained for the bio-electrode prepared using the ZnO:N ($x$ = 0.08) thin film matrix. Thus, nitrogen doping in ZnO has proved to be a simple, reliable and efficient way to improve the sensitivity of ZnO-based biosensors. The lower limit of detection (LOD) of the developed uric acid biosensor has been evaluated at a signal to noise ($S/N$) ratio of 3, and is found to be about 0.04 mM. The low detection limit suggests the high accuracy of the developed biosensor for the detection of uric acid. In addition, the prepared uricase/ZnO:N/ITO/glass biosensor has a fast response time of about 4 seconds. The obtained results suggest that the ZnO:N thin film acts as an excellent electron accelerator, resulting in a fast electron transfer between enzyme (uricase) and electrode.

In order to verify the affinity of the immobilized uricase molecule on the surface of the ZnO:N thin film matrix, the value of the Michaelis–Menten kinetic parameter ($K_m$) was estimated from the Hanes plot shown in inset (b) of Fig. 7. The estimated value of $K_m$ is about 0.10 mM which is relatively lower than the corresponding values reported in the range of 0.17–7.8 mM by other workers for uric acid biosensors.[12,50,51,56,57] The value of $K_m$ is also estimated using half maximal velocity and is found to be 0.10 mM which is in agreement with that obtained using the Hanes plot. The obtained low value of $K_m$ suggests that the ZnO:N ($x$ = 0.08) matrix provides a biocompatible environment to the enzyme (uricase) and is favourable to the orientation of the immobilized uricase molecule. This also highlights the high

affinity of the uricase/ZnO:N/ITO/glass bio-electrode towards uric acid.

### Photometric enzyme assay

In order to carry out the photometric assay, the uricase/ZnO:N/ITO/glass bio-electrode was dipped in 3 ml PBS solution containing HRP solution (1 mg $ml^{-1}$), 20 ml solution of *o*-dianisidine dye (1% in $H_2O$) (freshly prepared) and different concentrations of uric acid solution. The apparent enzyme activity, *i.e.* the concentration of enzyme active sites participating in the bio-chemical reaction per unit time, is then estimated using eqn (2)[58]

$$a_{app}^{enz}\ (U\ cm^{-2}) = AV/\varepsilon ts, \quad (2)$$

where $A$ is the difference in absorbance of the bio-electrode before and after incubation when saturation is achieved, $V$ is the total volume (3.17 $cm^3$), $\varepsilon$ is the millimolar extinction coefficient (7.5 for *o*-dianisidine at $\lambda = 500$ nm), $t$ is the reaction time (2 min) and $s$ is the surface area (1 $cm^2$) of the bio-electrode.[56] The difference between the initial and final absorbance values at a fixed wavelength ($\lambda = 500$ nm) corresponding to the absorption of *o*-dianisidine dye as a function of uric acid concentration is measured and is shown in Fig. 8. The enzyme activity increases linearly with increase in uric acid concentration up to 0.5 mM and shows a saturation tendency thereafter (Fig. 8). The apparent enzyme activity for the uricase/ZnO:N/ITO/glass bio-electrode is estimated to be $1.05 \times 10^{-2}$ U $cm^{-2}$, indicating that large units of uricase biomolecules are active on a unit surface area (1 $cm^2$) of the electrode.

### Effect of interferents on the biosensing response

Since various other metabolites such as glucose, cholesterol, urea *etc.* also coexist with uric acid in human blood, which may interfere with the uric acid biosensing response, the selectivity of the developed ZnO:N thin film-based biosensor towards uric acid was studied. This is carried out by monitoring the variation in the peak oxidation current in the cyclic voltammograms after the addition of different interferents (glucose (5 mM), cholesterol (5 mM), urea (1 mM), ascorbic acid (0.1 mM) and lactic acid (0.5 mM)) to the PBS solution containing 0.20 mM of uric acid.[21] The variation in peak oxidation current after the addition of interferents is shown in inset (a) of Fig. 8. The obtained results clearly demonstrate that there is no significant change in the measured current as a result of the tested interferents and that the presence of various interferents has a negligible effect on the biosensing response of the uricase/ZnO:N/ITO/glass bio-electrode towards uric acid. Thus, it is inferred that the prepared bio-electrode based on the ZnO:N thin film is capable of the selective and sensitive determination of uric acid.

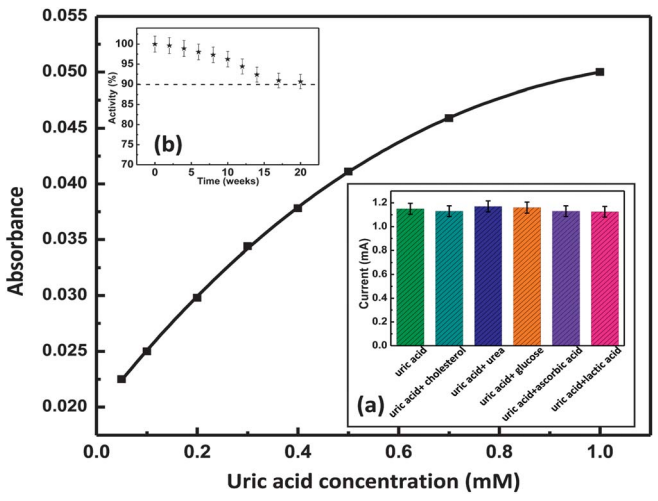


**Fig. 8** Photometric assay of the uricase/ZnO:N/ITO/glass bio-electrode as a function of uric acid concentration. Inset (a) gives the effect of other interferents present in serum on the biosensing response of the uricase/ZnO:N/ITO/glass bio-electrode. Inset (b) shows the shelf-life study of the prepared uricase/ZnO:N/ITO/glass bio-electrode.

### Stability of the uricase/ZnO:N/ITO/glass bio-electrode

The long-term stability of the prepared uric acid biosensor has been investigated over a period of 5 months by measuring the electrochemical current response of the prepared biosensor after regular time intervals (15 days). The test concentration of uric acid in the stability study was kept at 0.20 mM and the current was normalized with the peak current obtained when the biosensor was used for the first time. Degradation was studied with respect to this current when the biosensor was stored for some time. Inset (b) of Fig. 8 gives the variation in the activity of the bio-electrode as a function of time. It is observed (inset (b) of Fig. 8) that the biosensor retains more than 90% of its activity even after 20 weeks when stored at 4 °C, demonstrating the high shelf-life of the developed bio-electrode. The shelf-life of the prepared biosensor is higher than other bio-electrodes developed for uric acid biosensing using various matrices such as polyelectrolyte multilayers, 30 days;[59] ZnO nanorods, 20 days;[51] polyaniline, 60 days;[7] Ir-modified carbon, 10 days;[4] eggshell membrane, 90 days;[57] nano-Au/PPyox, 30 days;[11] quercetin-modified WGE, 30 days;[16] epoxy resin membrane, 60 days;[56] SAM of APTES, 50 days;[1] and ZnO NWs, 21 days.[17] The high shelf-life of the prepared bio-electrode may be attributed to the high stability and excellent biological compatibility of the nitrogen-doped ZnO thin film grown by the physical deposition technique (PLD) which provided a good microenvironment for the enzyme to maintain its activity. It may be noted that the entire set of CV measurements to determine the calibration curve was repeated 3 times and the repeated measurement results were found to lie close to each other without deviations. The error in the repeated cycles was found to be around 5% in the entire range. For lower values of currents, ±5% gives less deviation compared to higher values of current. So, on the same scale, low currents result in smaller error bars which increase for high currents. The experiment was also performed for new devices fabricated with the similar conditions under different batches as well and similar results were found to be within the experimental errors.

**Table 3** Determination of uric acid in real serum samples using the proposed biosensor

| Real serum sample | Content of uric acid measured/mM | | R.S.D. of developed biosensor ($n = 6$) (%) | Spike/mM | Concentration of uric acid detected/mM | Recovery (%) | R.S.D. of developed biosensor ($n = 6$) (%) |
|---|---|---|---|---|---|---|---|
| | Uricase/ZnO:N/ITO/glass bio-electrode | Spectrophotometric method | | | | | |
| 1 | 0.156 | 0.160 | 1.5 | 0.3 | 0.450 | 98 | 1.1 |
| 2 | 0.251 | 0.243 | 1.9 | 0.3 | 0.554 | 101 | 1.4 |
| 3 | 0.475 | 0.481 | 1.2 | 0.3 | 0.773 | 99.3 | 1.3 |

### Real sample analysis

In order to demonstrate the practical utility of the developed ZnO:N thin film-based biosensor, the prepared bio-electrode was applied to determine the concentration of uric acid in three human serum samples. The current response obtained from CV measurements after the addition of serum in the electrolyte solution was obtained. The uric acid concentration in serum was then extrapolated from the standard calibration curve between uric acid concentration and current (inset (a) of Fig. 7). To validate the accuracy, the content of uric acid in serum samples determined by the prepared biosensor was compared with that measured by a commercial spectrophotometric method in the clinical laboratory. The results obtained are presented in Table 3. The results of this present work are in close agreement with the corresponding values obtained from the clinical lab using spectrophotometric techniques (not shown here). In order to demonstrate the accuracy and precision of the biosensor, recovery tests were also performed by adding a known concentration of uric acid (0.30 mM) in the already tested serum samples and then estimating the concentration of the added uric acid (Table 3). The performed recovery tests confirm that the fabricated biosensor based on the ZnO:N thin film matrix is accurate and precise. The reproducibility and reliability of the present biosensor was examined by determining the uric acid content in the same serum sample (sample 1, Table 3) six times a day (within day) and after their one-week of storage at −20 °C (between day). The coefficient of variation (CV) values of the biosensor within- and between-day were about 2.5 and 3.0%, respectively, which highlights the excellent performance of the uricase/ZnO:N/ITO/glass bio-electrode.

## Conclusion

Nitrogen-doped ZnO (ZnO:N) thin film offers an efficient platform for the development of a uric acid biosensor with enhanced response in comparison to using the ZnO thin film alone. The introduction of defect states upon N doping makes ZnO:N an attractive matrix with excellent charge transfer characteristics. The nanocrystalline morphology of the prepared matrix increases the surface-to-volume ratio, thus providing a comparatively high sensitivity (1.1 mA $mM^{-1}$ $cm^{-2}$) towards uric acid. The biosensing response of the prepared sensor is linear over a wide detection range (0.05–1.0 mM). The low $K_m$ value of 0.10 mM indicates the high affinity of uricase immobilized on the surface of the ZnO:N thin film towards uric acid. The developed ZnO:N (8% N doped) thin film biosensor is stable for a period of 20 weeks. The prepared uricase/ZnO:N/ITO/glass biosensor has been successfully employed to determine the level of uric acid in human serum.

## Acknowledgements

Authors are thankful to the Department of Science and Technology (DST) for the financial support to carry out the proposed work. One of the authors (K.J.) acknowledges UGC and University of Delhi for research fellowship. We are also thankful to St. Stephens hospital for providing real serum samples for the present study. Authors acknowledge Dr. Rita Singh, Department of Zoology, University of Delhi for fruitful discussions and all the help.

## References

1 T. Ahuja, Rajesh, D. Kumar, V. K. Tanwar, V. Sharma, A. M. Biradar and N. Singh, *Thin Solid Films*, 2010, **519**, 1128–1134.
2 J. Yu, S. Wang, L. Ge and S. Ge, *Biosens. Bioelectron.*, 2011, **26**, 3284–3289.
3 D. Martinez-Pérez, M. L. Ferrer and C. R. Mateo, *Anal. Biochem.*, 2003, **322**, 238–242.
4 Y. C. Luo, J. S. Do and C. Liu, *Biosens. Bioelectron.*, 2006, **22**, 482–488.
5 M. Tyagi, M. Tomar and V. Gupta, *Biosens. Bioelectron.*, 2013, **41**, 110–115.
6 M. M. Castillo-Ortega, D. E. Rodriguez, J. C. Encinas, M. Plascencia, F. A. Mendez-Velarde and R. Olayo, *Sens. Actuators, B*, 2002, **85**, 19–25.
7 J. Kan, X. Pan and C. Chen, *Biosens. Bioelectron.*, 2004, **19**, 1635–1640.
8 F. Arslan, *Sensors*, 2008, **8**, 5492–5500.
9 X. Y. Wang, T. Hagiwara and S. Uchiyama, *Anal. Chim. Acta*, 2007, **1**, 41–46.
10 S. Cete, A. Yasar and F. Arslan, *Artif. Cells, Blood Substitutes, Immobilization Biotechnol.*, 2006, **34**, 367–380.
11 J. Li and X. Q. Lin, *Anal. Chim. Acta*, 2007, **596**, 222–230.
12 Y. Jiang, A. Wang and J. Kan, *Sens. Actuators, B*, 2007, **124**, 529–534.
13 M. Bhambi, G. Sumana, B. D. Malhotra and C. S. Pundir, *Artif. Cells, Blood Substitutes, Immobilization Biotechnol.*, 2010, **38**, 178–185.
14 P. Y. Chen, R. Vittal, P. C. Nien, G. S. Liou and K. C. Ho, *Talanta*, 2010, **80**, 1145–1151.

15 X. Pan, S. Zhou, C. Chen and J. Kan, *Sens. Actuators, B*, 2006, **113**, 329–334.
16 J. B. He, G. P. Jin, Q. Z. Chen and Y. Wang, *Anal. Chim. Acta*, 2007, **585**, 337–343.
17 S. M. U. Ali, N. H. Alvi, Z. Ibupoto, O. Nur, M. Willandera and B. Danielsson, *Sens. Actuators, B*, 2011, **152**, 241–247.
18 H. K. Yadav, V. Gupta, K. Sreenivas, S. P. Singh, B. Sundarakannan and R. S. Katiyar, *Phys. Rev. Lett.*, 2006, **97**, 085502.
19 N. Batra, M. Tomar and V. Gupta, *Analyst*, 2012, **137**, 5854.
20 S. Saha and V. Gupta, *J. Appl. Phys.*, 2011, **110**, 064904.
21 J. Singh, P. Kalita, M. K. Singh and B. D. Malhotra, *Appl. Phys. Lett.*, 2011, **98**, 123702.
22 Z. Yang, X. Zong, Z. Ye, B. Zhao, Q. Wang and P. Wang, *Biomaterials*, 2010, **31**, 3534–3541.
23 J. Wang, S. Li and Y. Zhang, *Electrochim. Acta*, 2010, **55**, 4436–4440.
24 S. M. U. Ali, Z. H. Ibupoto, S. Salman, O. Nur, M. Willander and B. Danielsson, *Sens. Actuators, B*, 2011, **160**, 637–643.
25 X. Liu, P. Lin, X. Yan, Z. Kang, Y. Zhao, Y. Lei, C. Li, H. Du and Y. Zhang, *Sens. Actuators, B*, 2013, **176**, 22–27.
26 M. Tyagi, M. Tomar and V. Gupta, *Anal. Chim. Acta*, 2012, **726**, 93–101.
27 M. Das, G. Sumana, R. Nagarajan and B. D. Malhotra, *Appl. Phys. Lett.*, 2010, **96**, 133703.
28 R. Devi, M. Thakur and C. S. Pundir, *Biosens. Bioelectron.*, 2011, **26**, 3420–3426.
29 S. Yadav, R. Devi, A. Kumar and C. S. Pundir, *Biosens. Bioelectron.*, 2011, **28**, 64–70.
30 J. G. Lu, Y. Z. Zhang, Z. Z. Ye, Y. J. Zeng, H. P. He, L. P. Zhu, J. Y. Huang, L. Wang, J. Yuan, B. H. Zhao and X. H. Li, *Appl. Phys. Lett.*, 2006, **89**, 112113.
31 H. K. Yadav, K. Sreenivas, V. Gupta and R. S. Katiyar, *J. Appl. Phys.*, 2008, **104**, 053507.
32 O. Lupan, L. Chowa, T. Pauporté, L. K. Ono, B. R. Cuenya and G. Chai, *Sens. Actuators, B*, 2012, **173**, 772–780.
33 J. C. Fan, C. Y. Zhu, S. Fung, Y. C. Zhong, K. S. Wong, Z. Xie, G. Brauer, W. Anwand, W. Skorupa, C. K. To, B. Yang, C. D. Beling and C. C. Ling, *J. Appl. Phys.*, 2009, **106**, 073709.
34 K. Y. Wu, Q. Q. Fang, W. N. Wang, C. Zhou, W. J. Huang, J. G. Li, Q. R. Lv, Y. M. Liu, Q. P. Zhang and H. M. Zhang, *J. Appl. Phys.*, 2010, **108**, 063530.
35 R. D. Shannon, *Acta Crystallogr., Sect. A: Cryst. Phys., Diffr., Theor. Gen. Crystallogr.*, 1976, **32**, 751.
36 W. W. Liu, B. Yao, Z. Z. Zhang, Y. F. Li, B. H. Li, C. X. Shan, J. Y. Zhang, D. Z. Shen and X. W. Fan, *J. Appl. Phys.*, 2011, **109**, 093518.
37 A. P. Bhirud, S. D. Sathaye, R. P. Waichal, L. K. Nikam and B. B. Kale, *Green Chem.*, 2012, **14**, 2790.
38 Y. H. Chou, J. L. H. Chau, W. L. Wang, C. S. Chen, S. H. Wang and C. C. Yang, *Bull. Mater. Sci.*, 2011, **34**, 477–482.
39 V. B. Raj, A. T. Nimal, Y. Parmar, M. U. Sharma and V. Gupta, *Sens. Actuators, B*, 2012, **166–167**, 576–585.
40 Y. Cao, L. Miao, S. Tanemura, M. Tanemura, Y. Kuno and Y. Hayashi, *Appl. Phys. Lett.*, 2006, **88**, 251116.
41 K. Jindal, M. Tomar and V. Gupta, *J. Appl. Phys.*, 2012, **111**, 102805.
42 B. Ma, G. K. L. Goh, J. Ma and T. J. White, *J. Electrochem. Soc.*, 2007, **154**(10), D557–D561.
43 I. Ozgur Ozer, E. Suvaci and S. Bernik, *Acta Mater.*, 2010, **58**, 4126–4136.
44 O. Lupan, T. Pauporté, I. M. Tiginyanu, V. V. Ursaki, V. Şontea, L. K. Ono, B. Roldan Cuenya and L. Chow, *Thin Solid Films*, 2011, **519**, 7738–7749.
45 D. D. Deligianni, N. Katsala, S. Ladas, D. Sotiropoulou, J. Amedee and Y. F. Missirlis, *Biomaterials*, 2001, **22**, 1241–1251.
46 R. Chen, C. Huang, Q. Ke, C. He, H. Wang and X. Mo, *Colloids Surf., B*, 2010, **79**, 315–325.
47 M. L. Addonizio, A. Castaldo, A. Antonaia, E. Gambale and L. Iemmo, *J. Vac. Sci. Technol., A*, 2012, **30**, 031506.
48 P. Li, S. H. Deng, Y. B. Li, L. Zhang, G. H. Liu and J. Huang, *Chin. J. Chem. Phys.*, 2012, **25**, 48–52.
49 R. Menon, V. Gupta, H. H. Tan, K. Sreenivas and C. Jagadish, *J. Appl. Phys.*, 2011, **109**, 064905.
50 S. Behera and C. R. Raj, *Biosens. Bioelectron.*, 2007, **23**, 556–561.
51 F. Zhang, X. Wang, S. Ai, Z. Sun, Q. Wan, Z. Zhu, Y. Xian, L. Jin and K. Yamamoto, *Anal. Chim. Acta*, 2004, **519**, 155–160.
52 Z. Matharu, P. Pandey, M. K. Pandey, V. Gupta and B. D. Malhotra, *Electroanalysis*, 2009, **21**, 1587–1596.
53 K. Arora, M. Tomar and V. Gupta, *Biosens. Bioelectron.*, 2011, **30**, 333–336.
54 B. Thakur and S. N. Sawant, *ChemPlusChem*, 2013, **78**, 166–174.
55 Z. Matharu, P. Pandey, M. K. Pandey, V. Gupta and B. D. Malhotra, *Electroanalysis*, 2009, **21**, 1587–1596.
56 J. Arora, S. Nandwani, M. Bhambi and C. S. Pundir, *Anal. Chim. Acta*, 2009, **647**, 195–201.
57 Y. Zhang, G. Wen, Y. Zhou, S. Shuang, C. Dong and M. M. F. Choi, *Biosens. Bioelectron.*, 2007, **22**, 1791–1797.
58 S. Saha, S. K. Arya, S. P. Singh, K. Sreenivas, B. D. Malhotra and V. Gupta, *Biosens. Bioelectron.*, 2009, **24**, 2040–2045.
59 T. Hoshi, H. Saiki and J. Anzai, *Talanta*, 2003, **61**, 363–368.

 